Communications Research Centre

DETECTION OF NEAR-EARTH TARGETS BY SPACE-BASED RADAR: DEVELOPMENT AND USE OF COMPUTER SIMULATIONS

by

B.J. Rook, J.S. Bird and A.W. Bridgewater

This work was sponsored by the Department of National Defence, Research and Development Branch under Project No. 33C87.

of Canada
of Communications
Gouvernement du Canada
Ministère des Communications

CRC REPORT NO. 1389
OTTAWA, JULY 1985

Canada

COMMUNICATIONS RESEARCH CENTRE

DEPARTMENT OF COMMUNICATIONS
CANADA

DETECTION OF NEAR-EARTH TARGETS BY SPACE-BASED RADAR: DEVELOPMENT AND USE OF COMPUTER SIMULATIONS

by

B.J. Rook, J.S. Bird and A.W. Bridgewater

(Radar and Communications Technology Branch)

CRC REPORT NO. 1389

July 1985
OTTAWA

This work was sponsored by the Department of National Defence, Research and Development Branch under Project No. 33C87.

TABLE OF CONTENTS

Page

DETECTION OF NEAR-EARTH TARGETS BY SPACE-BASED RADAR: DEVELOPMENT AND USE OF COMPUTER SIMULATIONS

by
B.J. Rook, J.S. Bird and A.W. Bridgewater

ABSTRACT

A time-based computer simulation of space-based radar (SBR) systems is described. This simulator models the orbital dynamics of multiple radar satellites and the characteristics of the radar, and computes the clutter returns from the surface of the Earth as a function of Doppler velocity. It then determines the theoretical detectability of a target of specified radar cross-section, location and velocity at any given time.

The simulator has been used to carry out studies of the detection performance of a generic SBR system in a low-altitude polar orbit using near-earth targets in the presence of earth clutter. The results from these studies show that (1) the detection performance varies according to look-direction, and (2) the detection probabilities, in general, decrease with decreasing target latitude.

1.0 INTRODUCTION

Since the advent of the satellite, there has been an increasing interest in the possibility of using a constellation of non-geostationary satellites for space-based radar surveillance and tracking. The fundamental advantages of such a system are (1) a greatly increased field-of-view, (2) a twenty-four hour capability regardless of weather conditions and (3), except for very low grazing angles, a direct line-of-sight regardless of terrain type. With these advantages, an SBR system could provide continuous surveillance of the Earth's surface including areas denied to other radar systems for political or geographical reasons. The disadvantage of SBR is that since its field-of-view is much greater than that of conventional ground-based radars, it is much more susceptible to countermeasures.

In this report, we develop the necessary mathematics to describe the dynamics, geometry and the radar design parameters of multiple radar satellites orbiting about a rotating Earth. In addition, a mathematical description is given of the clutter returns from the surface of the Earth based on the results of [6]. These mathematical equations have been converted to a discrete number representation in a digital computer to simulate SBR systems and the physical environment in which they operate.

A time-based simulator has been used to carry out studies of the detection performance of a generic low-altitude radar satellite in the

presence of earth clutter using near-earth targets. Although the studies have been restricted to the simulation of one radar satellite, with a single set of radar parameters and operating in a circular polar orbit, the simulator can readily model a constellation of radar satellites in multiple orbits and configurations and employ any desired radar system parameters.

2. SATELLITE DYNAMICS AND GEOMETRY

In this section, the necessary dynamical and geometrical relationships of orbiting satellites are developed for the investigation of space-based radar performance. In this development, it is assumed that the radar satellite moves in an ideal Keplerian orbit about a spherical Earth.

2.1 Dynamics of Orbiting Satellites

The general elliptical orbit of the satellite is illustrated in fig.(1). The origin of the coordinates is at the force centre F which corresponds to the centre of the Earth. The x_1-axis is chosen to lie in a direction from F to P, the pericentre of the ellipse. The position of the satellite S, is described in plane polar coordinates (r,θ) as shown. In polar coordinates (r,θ), the position and motion of the satellite are described by the following equations[1]:

$$r = \frac{h^2/\mu}{1 + e \cos f} = \frac{a(1 - e^2)}{1 + e \cos f} \quad , \tag{1}$$

$$\theta = f \quad , \tag{2}$$

$$\dot{r} = (he \sin f)/a(1 - e^2) \quad , \tag{3}$$

$$\dot{f} = \frac{h}{r^2} \tag{4}$$

where,

r is the radial distance;

f is the true anomaly;

e is the eccentricity of the ellipse;

a is the semi-major axis of the ellipse;

μ is the gravitational constant of the Earth normally taken to be 3.986008×10^{14} m^3/sec^2;

h is the angular momentum constant.

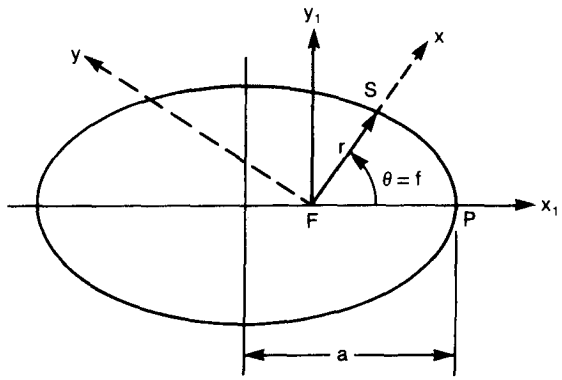

Figure 1 - Diagram defining the quantities to describe an elliptical orbit.

In order to calculate r and f as functions of time t, it is first necessary to solve the transcendental Kepler's equation for E, the eccentric anomaly[2], given a and e:

$$\overline{\omega}_s(t - T) = E - e \sin E \qquad (5)$$

where $\overline{\omega}_s = \left[\frac{\mu}{a^3}\right]^{\frac{1}{2}}$ is the mean angular velocity of the satellite.

In eqn.(5), the constant T is determined by specifying the time origin of pericentre passage of the satellite. If time is measured from the instant when the satellite is at P, then T = 0. The angle f is calculated from E:

$$f = \arctan\left[\frac{(1 - e^2)^{\frac{1}{2}} \sin E}{\cos E - e}\right] . \qquad (6)$$

The radius r is obtained from eqn.(1).

The relationship between f and E is illustrated in the geometrical construction of fig.(1a). S is the instantaneous position of the satellite on the elliptical path described by the polar coordinates (r,f); b is the length of the semi-minor axis of the ellipse. Through the point S erect a perpendicular to the x_1-axis. Q is the intersection of the perpendicular with the circumscribed auxiliary circle about the ellipse as shown. The angle OOF, denoted E, is the eccentric anomaly. In eqn.(5), the quantity $\overline{\omega}_s(t - t)$, where (t - T) is the elapsed time between P and S, is the mean anomaly which is also related to E. Mathematical expressions of the relationship between $\overline{\omega}_s(t - T)$ and E, and between f and E may be developed from this geometry and lead to eqns.(5) and (6) respectively.

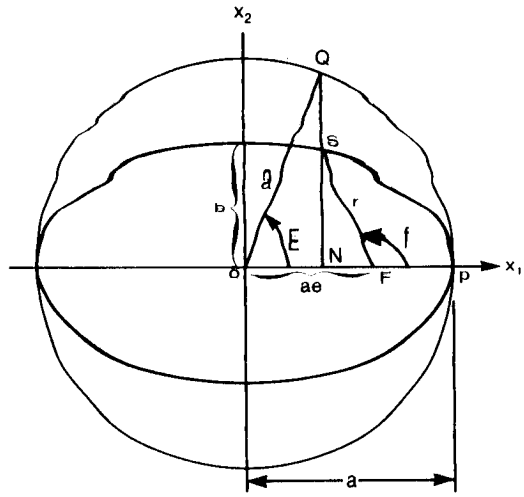

Figure 1a - Diagram illustrating the relationship between f and E.

2.2 Satellite Geometry in an Earth-Centred Coordinate System

The orientation of the orbital plane with respect to an earth-centred cartesian system of coordinates (X,Y,Z), rotating with the Earth, is shown in fig.(2). The X-axis is directed toward the Greenwich Meridian at the equator; the X-Y plane is the equatorial plane; the Z-axis is directed toward the geometric north pole; the z-axis is normal to the orbital plane. The definitions of the remaining symbols in the figure are as follows:

ω is the argument of the pericentre measured from the ascending node A to P;

i is the inclination angle of the orbital plane with respect to the reference equatorial plane;

λ_s is the longitude of the satellite;

δ_s is the latitude of the satellite;

Δ is an angle to be determined later;

Ω is the longitude of the ascending node given as a function of time by:

$$\Omega = \Omega_0 - \omega_e(t - T) \tag{7}$$

where,

Ω_0 is the initial longitude at time t = T;

ω_e is the angular velocity of the Earth normally taken to be 7.292115×10^{-5} radians/sec.

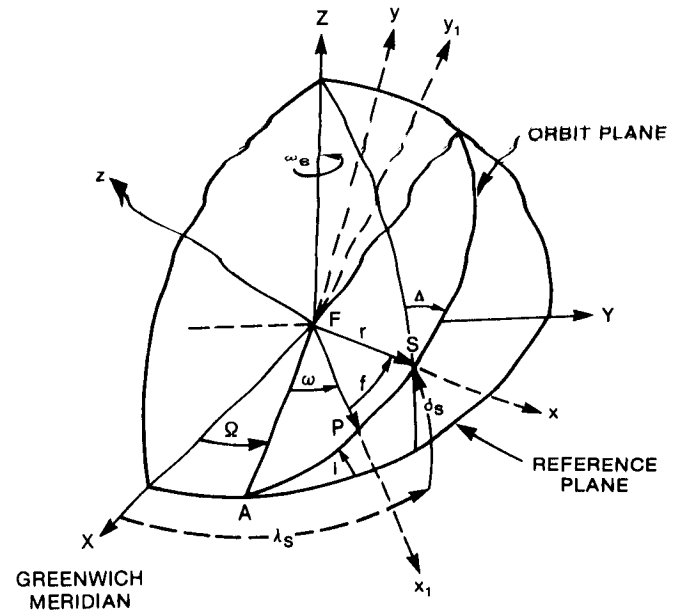

Figure 2 - Diagram illustrating the relationship between an orbital coordinate system and an earth-centred coordinate system.

The following transformation matrices for rotations about the three coordinate axes are defined:

$$R_1(\theta) = \begin{pmatrix} 1 & 0 & 0 \\ 0 & \cos\theta & \sin\theta \\ 0 & -\sin\theta & \cos\theta \end{pmatrix} \tag{8}$$

$$R_2(\theta) = \begin{pmatrix} \cos\theta & 0 & -\sin\theta \\ 0 & 1 & 0 \\ \sin\theta & 0 & \cos\theta \end{pmatrix} \tag{9}$$

$$R_3(\theta) = \begin{pmatrix} \cos\theta & \sin\theta & 0 \\ -\sin\theta & \cos\theta & 0 \\ 0 & 0 & 1 \end{pmatrix} \tag{10}$$

where $R_k(\theta)$, $k = 1,2,3$ represents an orthogonal matrix describing a counter-clockwise rotation about the kth axis by the angle θ as viewed from the positive end of the kth axis. Thus, $R_k(-\theta) = R_k^{-1}(\theta)$, where $R_k^{-1}(\theta)$ is the matrix inverse of $R_k(\theta)$, describes a clockwise rotation about the kth axis.

By a sequence of rotational transformations, the coordinates of the satellite's positional vector $\underline{r}_s$ in the (X,Y,Z) frame can be obtained from its coordinates in the rotating frame (x,y,z),

$$\begin{pmatrix} X_s \\ Y_s \\ Z_s \end{pmatrix} = R_3(-\Omega) \cdot R_1(-i) \cdot R_3(-u) \begin{pmatrix} r \\ 0 \\ 0 \end{pmatrix} \tag{11}$$

where

$$u = \omega + f \quad . \tag{12}$$

From eqn.(11), the longitude and latitude of the satellite are given by

$$\lambda_s = \arctan\left[\frac{Y_s}{X_s}\right] = \arctan\left[\frac{\cos u \sin \Omega + \sin u \cos i \cos \Omega}{\cos u \cos \Omega - \sin u \cos i \sin \Omega}\right] \tag{13}$$

and

$$\delta_s = \arcsin\left[\frac{Z_s}{r}\right] = \arcsin\left[\sin u \sin i\right] \quad , \tag{14}$$

which describes the position of the satellite, at some instant of time, in the geocentric coordinate system.

2.3 Velocity Components of the Satellite in an Earth-Centred Coordinate System

The components[3] of the satellite's velocity vector, denoted by $\dot{\underline{x}}$, may be written as,

$$\dot{\underline{x}} = \dot{r}\underline{\sigma} + r\dot{f}\underline{\rho} \tag{15}$$

where

$$\underline{\sigma} = \frac{\underline{r}}{r} \quad , \tag{16}$$

and $\underline{\rho}$ is a unit vector perpendicular to $\underline{\sigma}$ in the direction of increasing θ. The component $\dot{r}$, directed along the x-axis, is the velocity component due to the rate-of-change of the radius vector $\underline{r}$ and $r\dot{f}$, directed along the y-axis, is the velocity component of the satellite perpendicular to the radius vector. This coordinate system, which is shown in fig.(1), has been chosen to bring about the dependancy of $\dot{\underline{x}}$ on λ_s and δ_s.

If this coordinate system is rotated about the x-axis in a clockwise fashion by an amount $(\pi/2 - \Delta)$ to bring the z-axis into line with the Z-x plane (see fig.(2)) and the corresponding velocity component of the Earth, as a function of δ_s, is translated to the satellite and added, then the components of the velocity vector $\dot{\underline{r}}_s$ in the (X,Y,Z) frame are obtained by a sequence of rotational transformations:

$$\begin{pmatrix} \dot{X}_s \\ \dot{Y}_s \\ \dot{Z}_s \end{pmatrix} = R_3(-\lambda_s) \cdot R_2(\delta_s) \left\{ \begin{pmatrix} 0 \\ r\dot{\Omega} \cos \delta_s \\ 0 \end{pmatrix} + R_1(-[\pi/2 - \Delta]) \begin{pmatrix} \dot{r} \\ r\dot{f} \\ 0 \end{pmatrix} \right\}. \quad (17)$$

In eqn.(17), the addition of the two matrices inside the curly brackets results in a column matrix containing the components of the velocity vector of the satellite and that of the Earth translated to the satellite in a topocentric system. The origin of this system is considered to be coincident with that of the (X,Y,Z) frame.

In fig.(2), the angle Δ gives the instantaneous direction of motion of the satellite along the orbital path from S measured east of north from the latitudinal line as shown. The value of Δ may be determined by differentiating eqn.(14) with respect to u and taking the arc cos of the resultant:

$$\frac{d\delta_s}{du} = \frac{\cos u \sin i}{(1 - \sin^2 u \sin^2 i)^{\frac{1}{2}}} \quad (18)$$

from which

$$\Delta = \arccos \left[\pm \frac{\cos u \sin i}{(1 - \sin^2 u \sin^2 i)^{\frac{1}{2}}} \right] . \quad (19)$$

In eqn.(19), the positive sign indicates that the satellite is in an ascending node and the negative sign indicates that it is in a descending node. For example, if $i = \pi/2$, then $\Delta = 0$ or π indicating that when $\Delta = 0$, the satellite is ascending and when $\Delta = \pi$, the satellite is descending. From this example, it follows that for any inclination angle i, where $0 \leq i < \pi$, cos Δ will range between positive and negative values depending on whether the satellite is ascending or descending. For the special case of $i = 0$ (or π), cos $\Delta = 0$ for all u indicating that the satellite is neither ascending nor descending. For values of $i > \pi/2$, ambiguities arise in the calculation of Δ and therefore care must be taken when evaluating eqn.(19).

3. RADAR SATELLITE CONSTELLATION

A constellation of non-geostationary satellites may be used to provide continuous coverage of a point on or near the surface of the Earth[4]. The satellites may be arranged in single or multiple orbital planes using circular or elliptical orbits. The possible orientations of the satellites in the constellation are infinite. The simulation programme has the capability to deal with uniformly-distributed satellites in multiple uniformly-distributed orbits in order to permit future

studies to determine the most suitable radar-satellite constellation for the specified objectives of the SBR system.

3.1 Initial Angular Displacement

Let P be the specified number of orbital planes in the constellation and let Q be the specified number of satellites per plane. Thus, the total number of satellites, N, in the constellation is

$$N = P \cdot Q \quad . \tag{20}$$

At time t = T, the initial ascending node angle for the jth orbital plane relative to that of the first orbital plane may be given as

$$\Omega_j = \frac{\pi}{P}(j - 1), \; j = 1,2,3,.....P \quad . \tag{21}$$

The initial angular position of the kth satellite in the jth plane relative to that of the first satellite in the first orbital plane may be expressed in terms of Ω_j as

$$\alpha_{j,k} = [\Omega_j + 2\pi(k - 1)]/Q, \; k = 1,2,3,.....Q \quad , \tag{22}$$

thus,

$$\alpha_{j,k} = \frac{\pi(j - 1)}{N} + \frac{2\pi(k - 1)}{Q} \quad . \tag{23}$$

The first term on the right-hand side of eqn.(23) is an additional angle which is added to all the satellites in the jth plane so that none of the satellites in the constellation occupy the same point in space at any instant of time. Since from eqn.(20), Q = N/P, then eqn.(23) reduces to

$$\alpha_{j,k} = \frac{\pi}{N}\left[(j - 1) + 2P(k - 1)\right] \quad . \tag{24}$$

It should be noted from eqns.(21) and (24) that when j = k = 1, that is, the first satellite in the first orbital plane of the constellation, both Ω_j and $\alpha_{j,k}$ are equal to zero. Thus, for this satellite and plane, these two parameters, which are defined as Ω_0 and ω in Section 2.2, first must be specified before the initial angular positions of the remaining satellites can be calculated. In the following sub-sections, it will be shown how Ω_0 and ω are used in the process of computing the geometrical positions of the satellites in the constellation for any time t.

3.2 Equivalent Time Displacement

The values of Ω_j and $\alpha_{j,k}$ may be related to the period of rotation of the Earth and of the satellite orbit respectively to give

equivalent constant time displacements. Since ω_e is the angular velocity of the Earth and $\overline{\omega}_s$ is the average angular velocity of the satellite, then the ascending node angle for the jth plane expressed as an equivalent constant time displacement is

$$T_j = \frac{\Omega_j}{\omega_e} , \tag{25}$$

and the angular position of the kth satellite in the jth plane expressed as a constant time displacement is

$$T_{j,k} = \frac{\alpha_{j,k}}{\overline{\omega}_s} . \tag{26}$$

The variables $T_{j,k}$ are related to the initial positions of the satellites at t = T. The convention used is that $T_{1,1} = 0$ for the first satellite in the first plane which is at perigee at t = T. Thus, $T_{j,k}$ is the time lead of the j,kth satellite with respect to the 1,1th satellite; that is, the j,kth satellite was at perigee at a time $T - T_{j,k}$. In the following sub-section, it will be shown how these equivalent constant time displacements are used together with Ω_0 and ω in computing the geometrical positions of the satellites in the earth-centred coordinate system as a function of t using general elliptical orbits.

3.3 Geometrical Computations

From eqn.(25), the ascending node angle for the jth plane may be expressed in terms of ω_e and T_j, and may be used in eqn.(7) to give the jth nodal angle as a function of time t:

$$I_j = \Omega_j(t) = \Omega_0 - \omega_e(t - T_j - T) . \tag{27}$$

Similarly, from eqn.(26), $\alpha_{j,k}$ may be expressed in terms of $\overline{\omega}_s$ and $T_{j,k}$ and may be used in eqn.(5) giving

$$\overline{\omega}_s(t + T_{j,k} - T) = E_{j,k} - e \sin E_{j,k} \tag{28}$$

from which the angle $f_{j,k}$ is determined. This procedure allows for an even distribution of satellites in the orbital planes in a general elliptical orbit. Finally, the coordinates of the kth satellite in the jth orbital plane may be determined in the (X,Y,Z) frame by the use of eqn.(11) giving

$$\begin{pmatrix} X_{j,k} \\ Y_{j,k} \\ Z_{j,k} \end{pmatrix} = R_3(-I_j) \cdot R_1(-i) \cdot R_3(-u_{j,k}) \begin{pmatrix} r_{j,k} \\ 0 \\ 0 \end{pmatrix} \tag{26}$$

where,

$$u_{j,k} = \omega + f_{j,k} \tag{30}$$

and

$$r_{j,k} = \frac{a(1 - e^2)}{1 + e \cos f_{j,k}} \tag{31}$$

are both functions of t. It may be noted that the quantities a, e, Ω_0, ω, T and the inclination angle i are the same for all orbits in the constellation.

In fig.(3), an illustration is given of a constellation of eight satellites at heights of 4000 km above the Earth's surface; the constellation consisting of four circular polar-orbital planes with two satellites per plane, orbiting about a non-rotating Earth. The stars represent the positions of the satellites at some instant of time t. Seven of the eight satellites are in view at this instant of time.

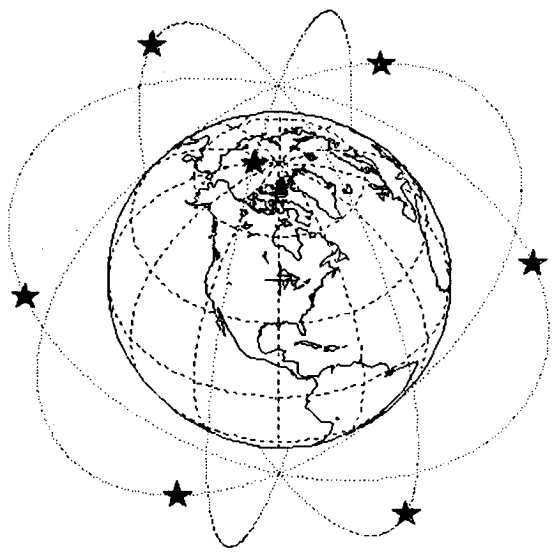

Figure 3 - Illustration of a constellation of eight satellites in circular polar orbits.

In the studies described in Section 10, only one radar satellite was necessary. However, the simulation facility provides for the specification of a constellation of satellites in the manner described above, and future studies will make use of this feature.

4.0 POSITION AND VELOCITY OF THE TARGET RELATIVE TO THE SATELLITE

In this section, a description is given of the position and velocity of a point target in an earth-centred rotating system of coordinates and in a local coordinate system centred at the satellite.

4.1 Position and Velocity of the Target in an Earth-Centred Coordinate System.

The position and velocity of the target are specified with respect to the Earth as shown in fig.(4) where

r_T is the radial distance of the target from the Earth's centre;
λ_T is the longitude of the target;
δ_T is the latitude of the target;
v_r is the rate-of-change of the radius vector (positive upward);
$v_e = v \sin B$ is the eastward component of the target velocity v;
$v_n = v \cos B$ is the northward component of the target velocity;

where B is the target heading angle measured east of north. A computer programme for target scenario generation has been written which calculates the sequence of position and velocity values for a number of specified targets, at regular intervals of time. This programme, which will be described in another report, can be linked to the SBR simulator to permit further analysis of detection and tracking techniques.

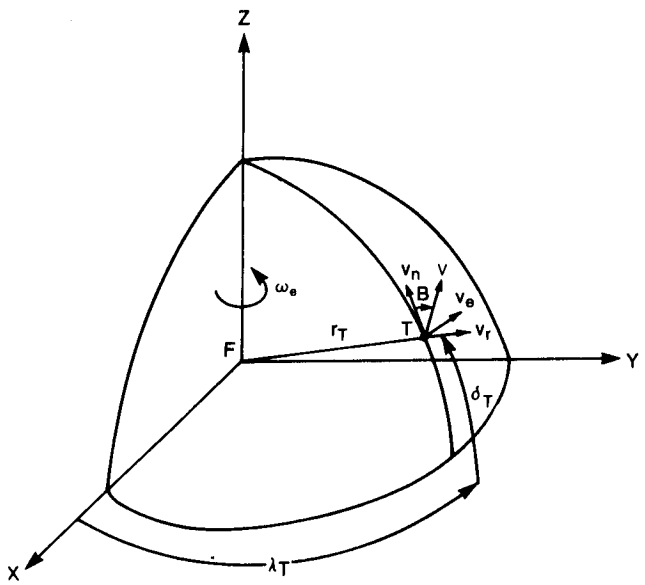

Figure 4 - Diagram illustrating the dynamics and geometry of the target in an earth-centred coordinate system.

If λ_T, δ_T and r_T have been specified, then the components of the target's positional vector $\underline{r}_T$ in the (X,Y,Z) frame may be given as

$$\begin{pmatrix} X_T \\ Y_T \\ Z_T \end{pmatrix} = R_3(-\lambda_T) \cdot R_2(\delta_T) \begin{pmatrix} r_T \\ 0 \\ 0 \end{pmatrix} . \qquad (32)$$

In a manner analogous to determining the satellite's velocity components in the (X,Y,Z) frame, the velocity components of the target's velocity vector $\underline{\dot{r}}_T$ in the (X,Y,Z) frame are

$$\begin{pmatrix} \dot{X}_T \\ \dot{Y}_T \\ \dot{Z}_T \end{pmatrix} = R_3(-\lambda_T) \cdot R_2(\delta_T) \begin{pmatrix} v_r \\ v_e \\ v_n \end{pmatrix} . \qquad (33)$$

4.2 Position of the Target Relative to the Satellite

The position of the target with respect to the satellite may be determined in topocentric spherical coordinates, that is, in range-angle coordinates centred at the satellite. The geometry of the situation is shown in fig.(5).

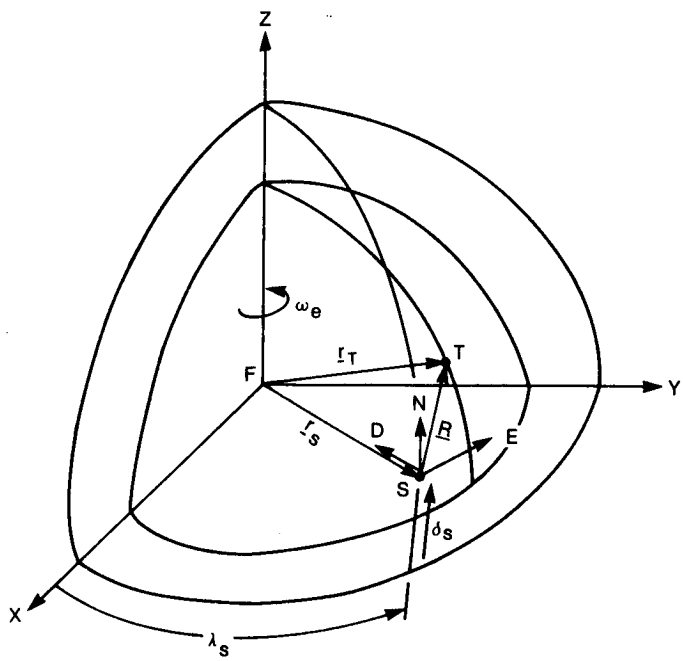

Figure 5 - Satellite-target geometry in the north-east-down coordinate system.

The range-angle coordinates are computed by first taking the vector difference between $\underline{r}_T$ and $\underline{r}_S$ and then rotating it into a North-East-Down (N,E,D) system of coordinates and carrying out the cartesian-to-spherical conversion:

$$\underline{R} = \underline{r}_T - \underline{r}_S \tag{34}$$

$$\begin{pmatrix} R_N \\ R_E \\ R_D \end{pmatrix} = R_2(-\pi/2-\delta_S) \cdot R_3(\lambda_S) \begin{pmatrix} R_X \\ R_Y \\ R_Z \end{pmatrix} \tag{35}$$

from which

$$R = \left(R_N^2 + R_E^2 + R_D^2\right)^{\frac{1}{2}} \tag{36}$$

is the slant range from the satellite to the target;

$$\phi_L = \text{arc tan } [R_E/R_N] \tag{37}$$

is the look-azimuth angle to the target, measured east of north;

$$\theta_L = \text{arc sin } [R_D/R] \tag{38}$$

is the look-down angle to the target, measured from the horizontal N-E plane. These coordinates are illustrated in fig.(5a).

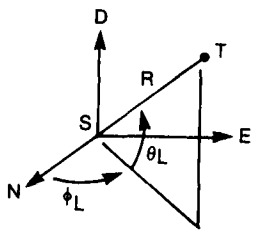

Figure 5a - Diagram of the N,E,D System Defining θ_L, ϕ_L and R.

4.3 Velocity Component of the Target Relative to the Satellite

The radial velocity component of the target with respect to the satellite is obtained by a similar process to that shown above, that is, by taking the vector difference $\dot{\underline{R}} = \dot{\underline{r}}_T - \dot{\underline{r}}_S$ and rotating it into the (N,E,D) system:

$$\begin{pmatrix} \dot{R}_N \\ \dot{R}_E \\ \dot{R}_D \end{pmatrix} = R_2(-\pi/2-\delta_s)\cdot R_3(\lambda_s)\begin{pmatrix} \dot{R}_X \\ \dot{R}_Y \\ \dot{R}_Z \end{pmatrix} \tag{39}$$

from which the rate-of-change of the slant range R is given by

$$\dot{R} = \frac{\dot{R}_N R_N + \dot{R}_E R_E + \dot{R}_D R_D}{R}$$

$$= \dot{R}_N \cos\phi_L \cos\theta_L + \dot{R}_E \sin\phi_L \cos\theta_L + \dot{R}_D \sin\theta_L \quad . \tag{40}$$

Since in this convention, negative values of $\dot{R}$ represents a closing target (a positive Doppler shift), then the radial velocity component V of the target as seen by the radar is normally defined as

$$V = -\dot{R} \quad . \tag{41}$$

4.4 Velocity of a Fixed Point on the Earth Relative to the Satellite

The relative velocity of a fixed point on the surface of the Earth due to a moving radar platform is of concern since it results in a Doppler shift on radar reflections from earth clutter. In this case, the clutter velocity vector $\dot{\underline{r}}_T$ is zero (here point clutter is treated as a target), and therefore the relative velocity of the point in the (N,E,D) local coordinate system is obtained by combining eqns.(17) and (39):

$$\begin{pmatrix} \dot{R}_N \\ \dot{R}_E \\ \dot{R}_D \end{pmatrix} = (-1)\begin{pmatrix} 0 & 0 & 1 \\ 0 & 1 & 0 \\ -1 & 0 & 0 \end{pmatrix}\begin{pmatrix} \dot{r} \\ r\dot{f}\cos(\pi/2 - \Delta) - r\omega_e \cos\delta_s \\ r\dot{f}\sin(\pi/2 - \Delta) \end{pmatrix} \tag{42}$$

$$= \begin{pmatrix} -r\dot{f}\cos\Delta \\ r\omega_e \cos\delta_s - r\dot{f}\sin\Delta \\ \dot{r} \end{pmatrix} \tag{43}$$

from which

$$\dot{R} = \left[r\omega_e \cos\delta_s \sin\phi_L - r\dot{f}\cos(\phi_L - \Delta)\right]\cos\theta_L + \dot{r}\sin\theta_L \quad . \tag{44}$$

The velocity of a point on the surface of the Earth relative to the satellite given by eqn.(44) may be expressed in terms of the grazing

angle γ instead of the look-down angle θ_L. In fig.(6) is shown the geometry of the earth-satellite relationship in the plane containing the Earth's centre and the slant range R from the satellite to the point on the Earth's surface. From the law of sines, the following relationships are available:

$$\frac{\sin(\theta_L - \gamma)}{R} = \frac{\cos\ \theta_L}{r_e} = \frac{\cos\ \gamma}{r} \tag{45}$$

where r_e is the radius of the Earth normally taken to be 6.378×10^6 metres. From these relationships, eqn.(44) may be rewritten giving

$$V = \left[V_{gs}\cos(\phi_L - \Delta) - V_e \cos\ \delta_s \sin\ \phi_L\right]\cos\ \gamma - \dot{r}\left[1 - \frac{r_e^2}{r^2}\cos^2\gamma\right]^{\frac{1}{2}} \tag{46}$$

where,

$V = -\dot{R}$ is the relative velocity of the point on the surface of the Earth with respect to the radar satellite,

$V_{gs} = r_e\dot{f}$ is the effective ground velocity of the satellite,

$V_e = r_e\omega_e$ is the rotational velocity of the Earth, and

where $\theta_L \leqslant \pi/2$ or alternatively $0 \leqslant \gamma \leqslant \pi/2$.

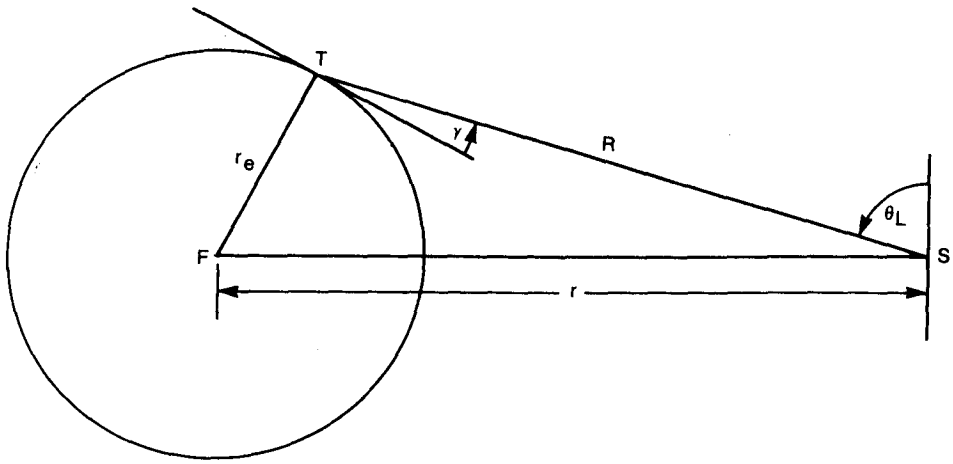

Figure 6 - Illustration of the earth-satellite geometry.

Equation (46) describes the velocity of a point on the surface of the Earth as seen by a radar satellite in a general elliptical orbit including the rotational velocity of the Earth as a function of the satel-

lite's latitudinal angle, δ_s. The equation is used later in calculating the magnitude and spectrum of earth-clutter (see Section 7.2).

5.0 DETERMINATION OF THE NORMALIZED ANTENNA RESPONSE

Equations for the normalized antenna response are given in the following sub-sections for both the uniformly-illuminated rectangular and elliptical apertures in terms of the antenna-centred coordinates. The relationship between the antenna-centred coordinates and the North-East-Down (N,E,D) satellite's local coordinate system is established by means of coordinate transformations. This allows the computation of the antenna response for any direction (θ,ϕ) and hence the inclusion of the earth-clutter returns weighted according to the normalized antenna response. The simulation always assumes that the boresight of the aperture is oriented in the look-direction of the target (θ_L,ϕ_L), which is the most favourable orientation for target detection.

5.1 Formulation of the Antenna Aperture Coordinate System

In the North-East-Down (N,E,D) local system of coordinates shown in fig.(7), a unit vector $\underline{r}$ in the direction (θ,ϕ) has components

$$\begin{pmatrix} r_N \\ r_E \\ r_D \end{pmatrix} = \begin{pmatrix} \cos\phi\cos\theta \\ \sin\phi\cos\theta \\ \sin\theta \end{pmatrix} . \qquad (47)$$

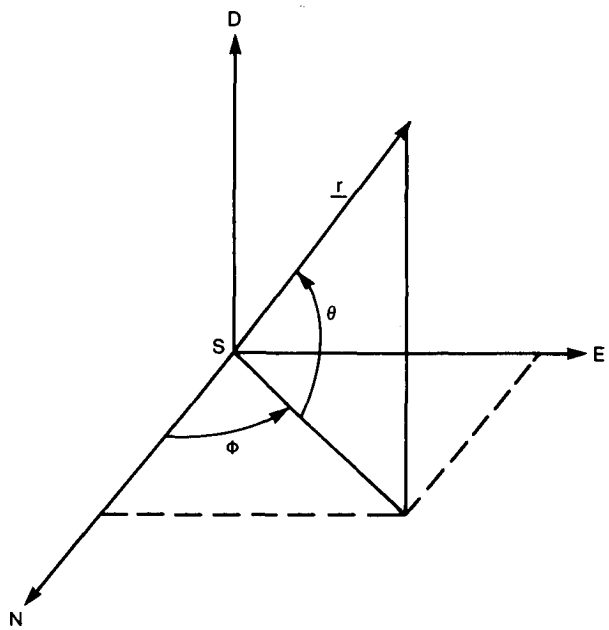

Figure 7 - Diagram of the spherical coordinates (θ,ϕ) in the North-East-Down coordinate system.

Rotate these components into the aperture coordinate system (x,y,z) such that the z-axis is aligned along the boresight of the aperture and the x-y plane is perpendicular to the boresight:

$$\begin{pmatrix} x \\ y \\ z \end{pmatrix} = R_2(\pi/2-\theta_L)\cdot R_3(\phi_L) \begin{pmatrix} r_N \\ r_E \\ r_D \end{pmatrix} . \tag{48}$$

Thus, in the (x,y,z) frame, shown in fig.(8), the x-y plane lies in the plane of the antenna aperture and the z-axis is perpendicular to that plane. After carrying out these rotations, the result is given in component form as

$$\begin{pmatrix} x \\ y \\ z \end{pmatrix} = \begin{pmatrix} \sin\theta_L \cos\theta \cos(\phi - \phi_L) - \cos\theta_L \sin\theta \\ \cos\theta \sin(\phi - \phi_L) \\ \cos\theta_L \cos\theta \cos(\phi - \phi_L) + \sin\theta_L \sin\theta \end{pmatrix} . \tag{49}$$

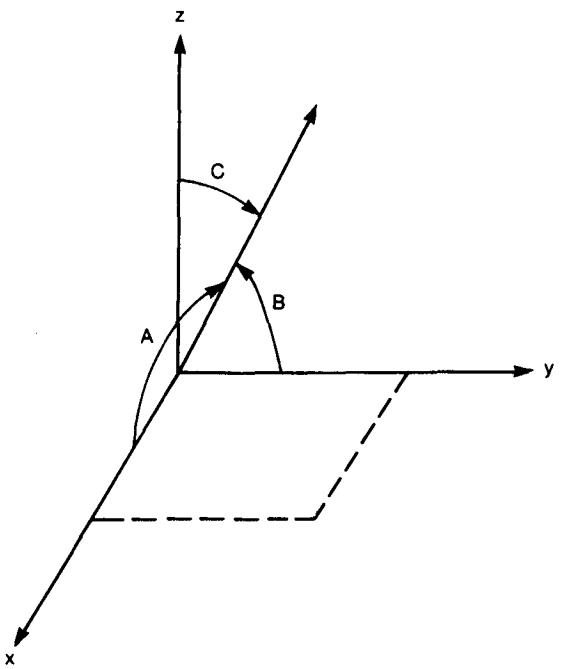

Figure 8 - Antenna aperture coordinate system.

In the aperture coordinate system shown in fig.(8), the cosines of the angles A, B and C are given by

$$\cos A = \sin\theta_L \cos\theta \cos(\phi - \phi_L) - \cos\theta_L \sin\theta \quad , \tag{50}$$

$$\cos B = \cos\theta \sin(\phi - \phi_L) \quad , \tag{51}$$

and

$$\cos C = \cos \theta_L \cos \theta \cos(\phi - \phi_L) + \sin \theta_L \sin \theta \quad . \qquad (52)$$

Thus, for fixed values of θ_L and ϕ_L, eqns.(50) - (52) are functions of θ and ϕ and may be used in determining the normalized antenna response for a specified type of aperture.

In the following sub-sections, equations for the responses of the rectangular and the elliptical apertures are presented. Equations for the responses of the square and circular apertures are obtained as special cases from the formulation for the responses of the rectangular and elliptical apertures.

5.2 Normalized Antenna Response for the Rectangular Aperture

Consider that the principal axes of the rectangular aperture are oriented along the (x-y) directions and that its boresight is perpendicular along the z-axis as shown in fig.(9). In this figure, the quantities a and b are the lengths of the semi-major and minor axes respectively. Thus, the normalized antenna power response for the rectangular aperture, $G_R(\theta,\phi)$, may be given as

$$G_R(\theta,\phi) = \left[\frac{\sin \left[\frac{2\pi}{\lambda} a \cos A\right]}{\frac{2\pi}{\lambda} a \cos A} \right]^2 \cdot \left[\frac{\sin \left[\frac{2\pi}{\lambda} b \cos B\right]}{\frac{2\pi}{\lambda} b \cos B} \right]^2 \qquad (53)$$

where λ is the wavelength.

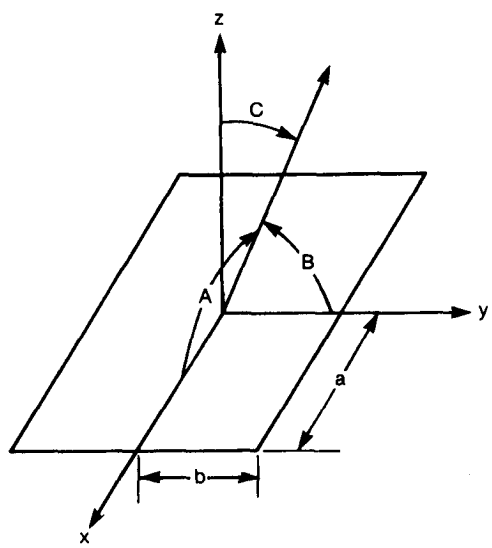

Figure 9 - Illustration of the rectangular aperture lying in the x-y plane of the antenna aperture coordinate system.

From eqn.(53), it follows that for the special case of a square aperture (a = b), its normalized response is given by

$$G_s(\theta,\phi) = \left[\frac{\sin\left[\frac{2\pi}{\lambda} a \cos A\right]}{\frac{2\pi}{\lambda} a \cos A}\right]^2 \cdot \left[\frac{\sin\left[\frac{2\pi}{\lambda} a \cos B\right]}{\frac{2\pi}{\lambda} a \cos B}\right]^2 . \quad (54)$$

5.3 Normalized Antenna Response for the Elliptical Aperture

For the elliptical aperture, a similar procedure is used for determining the normalized response. Consider that the principal axes of the ellipse are oriented along the (x-y) directions with its boresight perpendicular along the z-axis as shown in fig.(10). Again, the lengths of the semi-major and minor axes are given by the quantities a and b respectively. Thus, the normalized antenna power response for the elliptical aperture, $G_E(\theta,\phi)$, may be given as

$$G_E(\theta,\phi) = \left[\frac{2J_1\left[\frac{2\pi}{\lambda}\left(a^2\cos^2 A + b^2\cos^2 B\right)^{\frac{1}{2}}\right]}{\frac{2\pi}{\lambda}\left(a^2\cos^2 A + b^2\cos^2 B\right)^{\frac{1}{2}}}\right]^2 \quad (55)$$

where $J_1(X)$ is a first-order Bessel function.

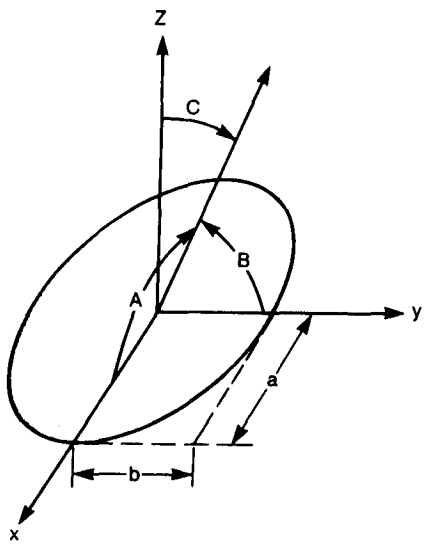

Figure 10 - Illustration of the elliptical aperture lying in the x-y plane of the antenna aperture coordinate system.

From eqn.(55), it follows that for the special case of a cicular aperture (a = b), the normalized response is given by,

$$G_c(\theta,\phi) = \left[\frac{2J_1\left[\frac{2\pi}{\lambda} a \left(\cos^2 A + \cos^2 B\right)^{\frac{1}{2}}\right]}{\frac{2\pi}{\lambda} a \left(\cos^2 A + \cos^2 B\right)^{\frac{1}{2}}} \right]^2 \quad . \tag{56}$$

Since

$$\cos^2 A + \cos^2 B = 1 - \cos^2 C = \sin^2 C \quad , \tag{57}$$

then eqn.(56) reduces to

$$G_c(\theta,\phi) = \left[\frac{2J_1\left[\frac{2\pi}{\lambda} a \sin C\right]}{\frac{2\pi}{\lambda} a \sin C} \right]^2 \quad . \tag{58}$$

6.0 SBR BASELINE SYSTEM DESIGN PRINCIPLES

The detection of targets near the surface of the Earth by an SBR system is difficult because radar echoes from targets are immersed in clutter echoes from the Earth. The latter can be very large because of the relatively large footprint of the antenna pattern and the unwanted contributions of earth clutter entering through the antenna sidelobes. Additionally, the very high velocity of the spacecraft results in a spread of clutter velocities creating difficulties for the separation of targets from clutter by Doppler filtering. In this section, basic radar system principles are discussed in the context of the SBR problem in order to facilitate the design of a baseline radar system. From studies with this baseline system, shortcomings can be noted and more sophistication added until the radar fully meets its specified objectives.

6.1 Constraints

Two major constraints govern the choice of an SBR waveform. As was mentioned above, earth-clutter returns can be very large with respect to target returns. High resolution Doppler processing is required to separate targets from clutter. However, targets cannot be separated if the Doppler velocities lie within a band of frequencies occupied by larger clutter returns. The band of frequencies occupied by the clutter defines a Minimum Detectable Velocity which cannot be allowed to become too large. This factor constrains the antenna aperture size and the antenna sidelobe levels. In addition to the clutter, a power resource problem exists because of the long operation ranges and restricted onboard power supplies. To provide the necessary Doppler resolution to overcome the clutter and the required energy to overcome system noise, a long-time coherent waveform is required combined with a large antenna aperture having sufficiently low sidelobe levels.

6.2 Radar Waveform Considerations

The waveform used in SBR is a compromise between range resolution and Doppler resolution[5]. It consists of a burst of pulses with each pulse modulated to improve the range resolution. In addition, the total burst is coherently processed to provide Doppler resolution. Since the peak power is limited on a radar satellite, the waveform has to be spread in time in order for the radar to receive the required signal energy for detection. Therefore, the duration of the pulse burst is a large fraction of the round-trip propagation time to the target. The duration of the pulse burst T_B limits the Doppler velocity resolution to

$$\Delta V = \frac{\lambda}{2T_B} \quad . \tag{59}$$

The pulse width τ of the individual pulses and the compression factor C_o limit the range resolution to

$$\Delta R = \frac{cC_o\tau}{2} \tag{60}$$

where c is the velocity of light. Ambiguous ranges arise as a result of the burst nature of the waveform. These ambiguous ranges are spaced about the true range at intervals which are inversely proportional to the pulse repetition frequency (PRF):

$$R_A = \frac{c}{2(PRF)} \quad . \tag{61}$$

Earth-clutter reflections are affected by these ambiguous ranges since each range and hence look-direction has a different Doppler frequency and antenna response. In the following section, it will be shown how these ambiguous ranges affect the earth-clutter returns.

7.0 DETECTION PERFORMANCE CALCULATIONS

In this section, the standard radar range and noise equations are used together with a mathematical description of the earth clutter to obtain a general signal-to-interference ratio which is used in determining system detection performance.

7.1 Calculation of Signal and Noise Levels

The signal and noise levels are calculated using the standard radar range and noise equations as follows:

$$S = \frac{N^2 P_K \tau G_L^2 \lambda^2 \sigma_T}{(4\pi)^3 R^4 L_s} \tag{62}$$

and

$$N_o = NKT_s \tag{63}$$

where,

N is the number of pulses in a burst;

P_k is the peak power;

τ is the pulse width;

G_L is the maximum antenna gain in the specified look-direction;

λ is the radar wavelength;

σ_T is the radar cross-section of the target;

R is the slant range;

L_s is the system loss;

K is Boltzman's constant;

T_s is the system noise temperature.

In the absence of clutter, these equations can be used to predict the performance of an SBR system and to study the effects on performance when the system parameters are varied.

7.2 Calculation of the Earth-Clutter Level

Calculating the earth-clutter level is a complicated problem because of its dependence on numerous parameters such as velocity, look-direction, antenna response, range ambiguities inherent in the waveform and the spherical shape of the Earth.

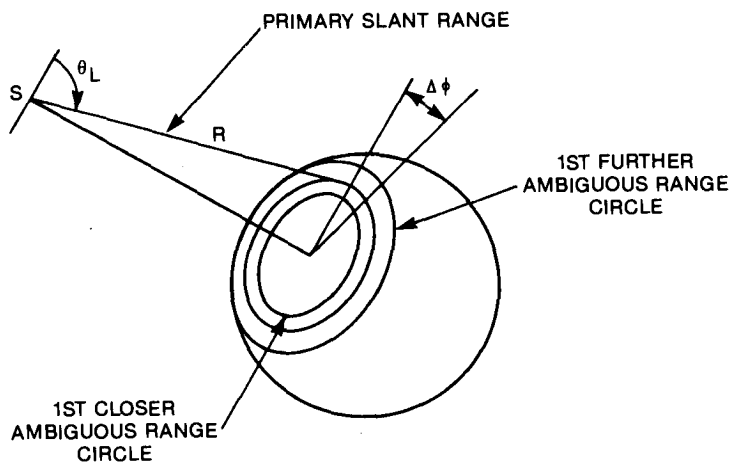

Figure 11 - Diagram illustrating the clutter element and ambiguous range circles on the surface of the Earth.

In order to picture the clutter problem, consider the illustra-

tion shown in fig.(11). A clutter return is received from a point on the surface of the Earth corresponding to the primary look-direction (θ_L, ϕ_L). This direction also corresponds to the look-direction of the target which is assumed to be located in the vicinity of the clutter point. This point has a certain Doppler frequency shift due to the relative velocity between the Earth and the satellite. In addition, clutter returns are received through the antenna sidelobes at other points on the constant primary-range circle. Further clutter returns are received from points on the constant ambiguous-range circles all with different relative velocities. The response for a single clutter element on the primary range circle at some arbitrary look-azimuth angle ϕ, may be given as

$$\Delta C(V) = \frac{P_k \tau G_L^2 \lambda^2}{L_s (4\pi)^3 R^4} N^2 \left[\frac{\tau c C_o R \cos \theta_L \, \Delta\phi}{2 \cos \gamma} \right] \sigma(\gamma) \, G^2(\theta_L, \phi) \qquad (64)$$

The factors inside the square brackets constitutes the area of the clutter element; $\Delta\phi$ is the angular width of the clutter element. The factor $\sigma(\gamma)$, is the clutter radar reflectivity. The factor $G(\theta_L, \phi)$ is the normalized antenna response relative to the maximum antenna gain G_L, oriented in the primary look-direction (θ_L, ϕ_L). In eqn.(64), it is assumed that the antenna gain does not change significantly over the angular extent of the single clutter element.

Each clutter element has its own velocity with respect to the satellite, therefore, only those elements with velocities which fall within the velocity bin of the signal processor will contribute to the clutter in the bin. Hence, the clutter level response may be expressed as[6]

$$C(V) = \frac{P_k \tau G_L^2 \lambda^2 \tau c C_o \Delta\phi}{2 L_s (4\pi)^3} \sum_{i \varepsilon I} \frac{W_i^2 \cos \theta_i \, \sigma(\gamma_i)}{R_i^3 \cos \gamma_i} G^2(\theta_i, \phi_i) \qquad (65)$$

where I is the set of all θ, ϕ and R that define the clutter elements which have the appropriate velocities, and W_i is a weight which depends on the range circle. For example, if a clutter element is on the primary range circle, $W_i = N$; if on the first closer or further circles, $W_i = N-1$ etc. Implicit in the calculation of C(V) are the angles θ and ϕ. These are determined by first specifying a velocity V within the velocity bin, and then solving eqn.(46) for θ and ϕ as shown in Appendix A. From these calculations, the normalized antenna response, given by the factor $G(\theta_i, \phi_i)$, may be determined relative to the maximum antenna gain G_L, assumed to be oriented in the primary look-direction (θ_L, ϕ_L), by first specifying the antenna aperture type and then carrying out the calculations as shown in Section 5.

7.3 Calculation of Signal-to-Interference Ratio

Expressions for signal, noise and clutter may be combined to form a general signal-to-interference ratio (SIR) calculation:

$$SIR = \frac{S}{I} = \frac{S}{N_o + C(V)} \tag{66}$$

where,

S is given by eqn.(62);

N_o is given by eqn.(63);

C(V) is given by eqn.(65);

$$I = N_o + C(V) \quad . \tag{67}$$

This ratio may be related to detection and false alarm probabilities through standard published curves [7] or direct calculations [8]. In eqn.(67), it is assumed that the quantities N_o and C(V) are independent and that N_o has Gaussian statistics.

8.0 SBR BASELINE SYSTEM PARAMETERS

In this section, representative numbers are applied to the design principles discussed previously in order to describe, in a quantitative manner, the performance of an SBR system.

To minimize the atmospheric attenuation of radar signals and the effects of radiation on the spacecraft, an L-band radar satellite (λ = 0.2m) at a height of 1000 km above the surface of the Earth in a circular polar orbit is the system considered. The objectve for the system is to detect a target near the surface of the Earth having a radar cross-section of -10.0 dBsm, with a probability of detection of 0.9 and a false alarm probability of less than 10^{-6}. This cross-section is chosen to reflect what might be considered as a lower limit of target radar cross-sections for detection by the radar. With these specified detection and false alarm probabilities, and with the assumption that two bursts are noncoherently added, the signal-to-interference ratio must be 14.8 dB. This value is obtained from Swerling's case 2 for fluctuating targets where the two bursts are at different radar frequencies. It is assumed that the range resolution is coarse enough so that the target remains within the range cell during the interval of the two bursts. Adding 3.0 dB to take account of cusping losses results in a minimum design signal-to-interference ratio of 17.8 dB.

The radar sensor used for the system is a uniformly-illuminated circular aperture of 70.0 metres in diameter. In addition, a peak power P_k, of 17.0 KW, a pulse length τ, of 50.0 μsec, a pulse repetition frequency (PRF), of 10 KHz and a compression factor C_o giving a range resolution ΔR, of 300.0 metres were chosen for the system. The system losses were assumed to amount to a total of 9.0 dB. The amplitude of the received radar signal was assumed to be uniformly weighted in time.

The values for antenna aperture size and pulse repetition frequency were chosen as a compromise to keep the peak power to a reasonable value and provide the necessary integration gain to overcome system noise at

the maximum range of interest. The value of the pulse length was chosen to give a duty cycle of 0.5. This is the maximum duty cycle allowable if each pulse in the burst is to be properly processed in the radar system's matched filter.

The system is required to detect the target out to a range of at least 3.390×10^6 metres corresponding to a grazing angle γ, of 3.0°. The length of the pulse burst T_B, is to equal the round-trip propagation time to the target. Thus, the total number of pulses in the burst N, for the specified (PRF) and the round-trip propagation time amounts to a value of 226.

In Table (1), a list is given of the radar parameters and shows the calculation of the signal-to-noise ratio, which is the signal-to-interference ratio in the absence of clutter. These parameters yield a designed SNR which exceeds the minimum required value of 17.8 dB provided the clutter levels are negligible. Some parameters, such as noise temperature T_s, have been arbitrarily chosen, but reflect current technology.

TABLE 1

Signal-to-Noise Ratio Calculation

	+ dB	- dB
$P_k\tau$ = 17.0 KWx50.0 μsec		0.71
$G_L^2 = \left[\frac{4\pi(\text{Area})}{\lambda^2}\right]^2$	121.65	
$\frac{\lambda^2}{(4\pi)^3}$		46.96
σ_T		10.00
$R^4(3.390\times10^6)^4$		261.21
$N^2(226)^2$	47.08	
KT_s	201.70	
N(226)		23.54
Losses		9.00
	370.43	351.42

Signal-to-noise ratio (SNR) = 370.43 - 351.42 = 19.01 dB

9.0 DETECTION PERFORMANCE IN THE PRESENCE OF EARTH-CLUTTER

In this section, results from the calculation of the signal-to-interference ratio as a function of velocity are presented to illustrate the variation in the clutter-velocity spectrum for different look-directions. Two look-down angles corresponding to grazing angles of 3.0° and 40.0° are considered. For these examples, the clutter-velocity spectrum is compared for two antenna orientations; $\phi_L = 0.0°$ corresponding to the look-ahead direction which is in line with the direction of motion of the satellite, and $\phi_L = 90.0°$ corresponding to a direction which is perpendicular to the direction of motion.

The radar-target range R varies with grazing angle γ for a given earth-satellite geometry (see fig.(6) and eqn.(45)). Therefore, the maximum available burst duration T_B and Doppler-velocity resolution ΔV also vary with γ (eqn.59)). For grazing angles of 3.0° and 40.0°, the velocity bin widths are 4.4 m/sec and 10.5 m/sec respectively.

For a particular velocity of interest, the clutter level is calculated from eqn.(65) from a knowledge of the velocity bin width, primary look-direction (θ_L, ϕ_L) and the latitude of the satellite. The calculation requires the solution of eqn.(46) for the appropriate θ_i and ϕ_i, as outlined in the Appendix. The signal-to-interference ratio is determinted by the use of eqn.(66).

For the results to be presented in the following sub-section, the latitude of the satellite was set to $\delta_s = 0.0°$ and assumed to be in an ascending node; the clutter reflectivity was set to a constant value of -20.0 dBsm. Although, in general, the value of the clutter reflectivity is dependent on grazing angle and terrain type, this dependency has not been included in the computer simulation at this time. Therefore, the value was chosen to reflect what might be considered as the average of the variations in the clutter reflectivity.

9.1 Performance Results

In this sub-section, results from the computation of the signal-to-interference ratio (SIR) as a function of velocity, relative to the velocity in the primary look-direction, are presented and examined. These results, therefore, serve to illustrate the detection performance of the system as a function of the radial velocity component of the target as observed by the radar satellite in the specified look-direction.

In fig.(12), a plot is given of the SIR against velocity for the grazing angle of 3.0° and look-azimuth angle of 0.0°. It is noted that for velocities in excess of 26.0 m/sec, there is a clear area in the spectrum in which the signal-to-interference ratio is limited only by system noise. This clear area arises as a result of the corresponding velocities appearing on range circles which are beyond the field-of-view of the radar satellite. The dashed line in the plot represents the threshold detection level of 17.8 dB. Targets for which the values of

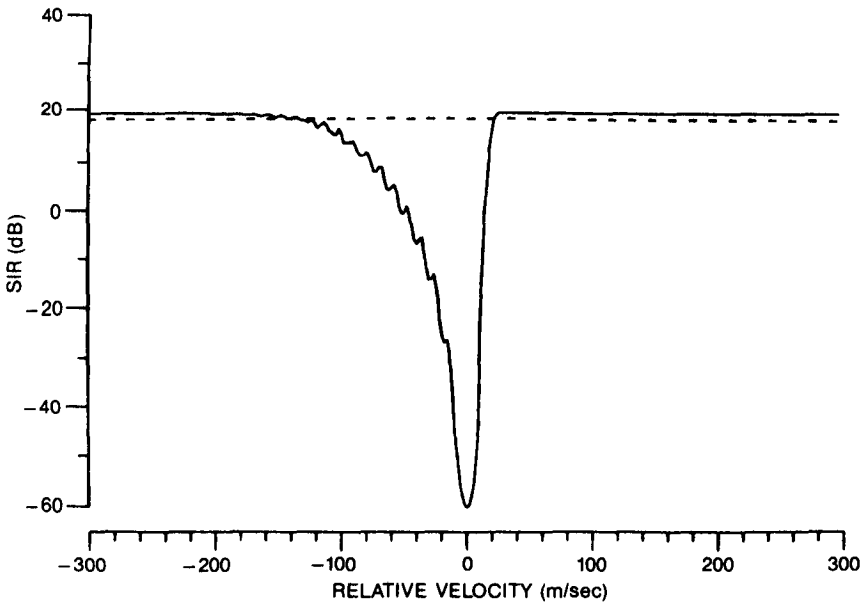

Figure 12 - Plot of the SIR against velocity, ϕ_L = 0.0°, γ = 3.0°

SIR fall below this level are assumed not detectable by the radar satellite. Note that targets having radial velocity components which fall inside the range from -132.0 m/sec to 24.0 m/sec are not detectable. These values are defined as the Minimum Detectable Velocities (MDV) of the system for this look-direction.

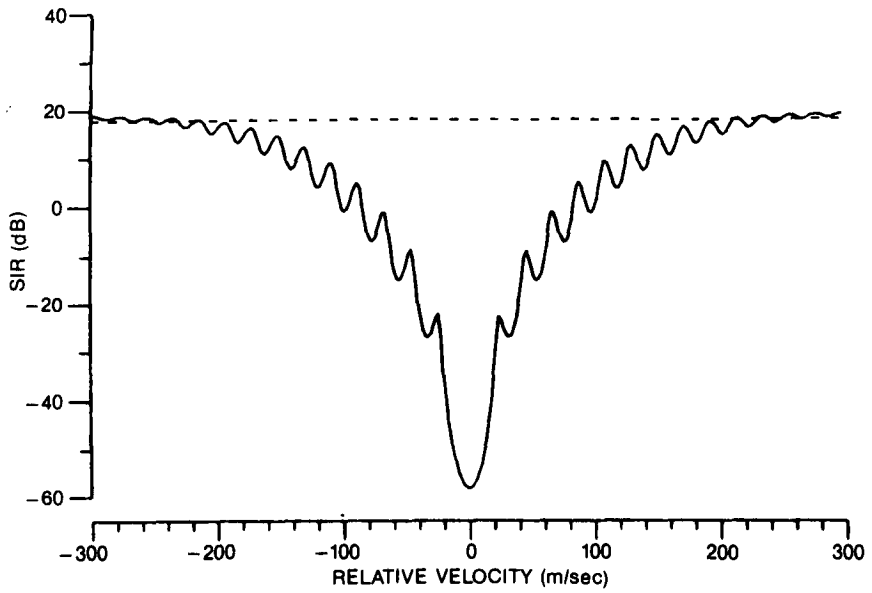

Figure 13 - Plot of the SIR against velocity, ϕ_L = 90.0°, γ = 3.0°.

In fig.(13), a plot is given of the SIR against velocity for the same grazing angle as before but now the look-azimuth angle is 90.0°. This result differs considerably from that of fig.(12) in that where before there was a clear area in the spectrum, it is now filled in. In addition, the spectrum is symmetrical about the relative velocity of zero. Again, for values of SIR which fall below the level of 17.8 dB, the corresponding targets are not detectable by the radar satellite. Note that targets having radial velocity components which fall inside the range from -252.0 m/sec to 252.0 m/sec are not detectable. Again, these are the MDV of the system for this look-direction. The large negative value of the MDV indicates a considerable spread in the clutter velocity spectrum compared to that in the look-ahead direction. These two results illustrate the extremes of the clutter spectrum at this grazing angle. For other values of ϕ_L, a partial filling in of the clear area arises together with an associated spread in the spectrum.

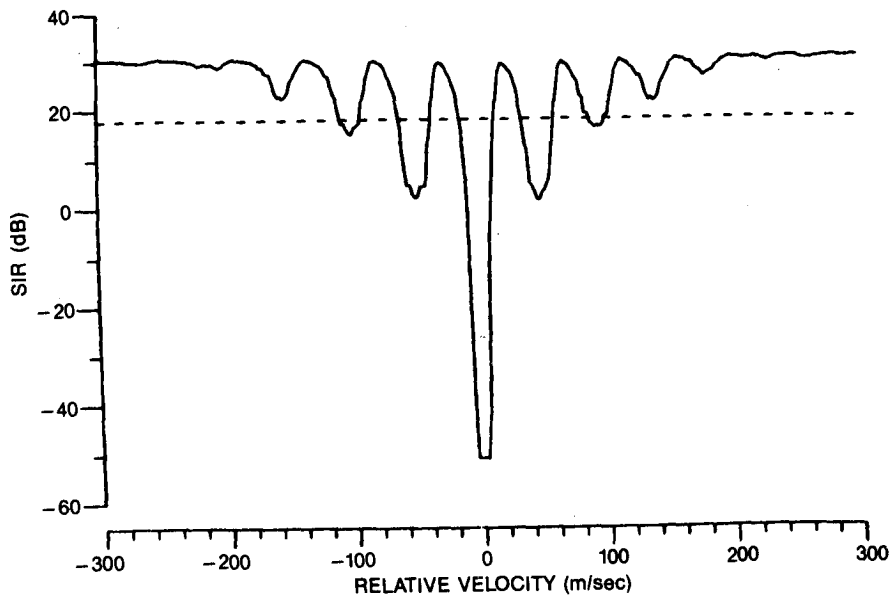

Figure 14 - Plot of the SIR against velocity, ϕ_L = 0.0°, γ = 40.0°.

In fig.(14), a plot is given of the SIR against velocity for a grazing angle of 40.0° and a look-azimuth angle of 0.0°. This result has a spiky appearance compared to the result of fig.(12) and is generally symmetrical about the relative velocity of zero. The values for the MDV are more difficult to determine in this result since the peaks of the curve cross over the threshold detection level several times. However, they might be considered to have values of -110.0 m/sec and 100.0 m/sec. For large positive and negative values of velocity, the signal-to-interference ratio is limited essentially by system noise, and is considerably greater than the designed signal-to-noise ratio owing to the shorter range at the increased grazing angle.

Comparing these three results, we observe that the clutter-velocity spectrum differs considerably from one look-direction to another. The curves shown in figs.(12) and (13) illustrate the extremes of the expected performance of the system when operating in a surveilance mode, and fig.(13) illustrates its expected performance when switched to a tracking mode. It has been found that these results are only slightly affected by the satellite's latitude δ_s, because the ground velocity of the satellite is so much greater than the velocity of the Earth.

10.0 DETECTION PROBABILITIES AS A FUNCTION OF TARGET HEADING AND LATITUDE

In the previous section, it was shown that the clutter-velocity spectrum varied significantly according to the look-direction. In this section, a description is given of a simulation scenario from which the detection probabilities of the SBR system, as a function of target latitude and heading, were calculated from measurements taken over all possible azimuth and look-down angles.

10.1 Simulation Scenario

The simulation scenario consisted of one SBR satellite orbiting the Earth in a circular polar orbit at a height of 1000 Km. The radar system parameters used were the same as those given in Section 8. The objective of the radar was to detect a target having a constant velocity of 150.0 m/sec, a constant height of 150.0 m, and a constant radar cross-section of -10.0 dBsm. The clutter reflectivity used was a constant -20.0 dBsm.

For each experiment, the satellite proceeded to orbit the Earth for a period corresponding to 48 hours. This afforded it the opportunity to "see" the target several thousand times over all possible azimuth and look-down angles. For each experiment, the target was fixed in position with respect to the Earth; its latitude and longitude never changed, however, the Earth rotated under the orbit of the satellite. For each experiment, the target's heading was held constant, and many experiments were carried out for different target headings and latitudes.

In the course of each experiment, the number of "possible detections" was accumulated, that is, the number of occasions (sampling interval of the time-based simulator) when the target was in line-of-sight of the radar-satellite. The number of "true detections" was also accumulated, that is, the number of occasions when the target's radial velocity component with respect to the radar was such that the target was theoretically detectable (SIR equalled or exceeded the 17.8 dB threshold). Thus, the detection probability as a function of target latitude and heading was calculated as the ratio of "true to possible" detections. It was assumed that the antenna always presented maximum aperture to the target. The results of these calculations are presented in the following sub-section.

10.2 Results

In fig.(15), plots are given of the detection probabilities as a function of heading angle for fixed target latitudes of 90.0° and 60.0°. These two results were chosen from numerous experimental results to illustrate certain features and trends in the simulated data.

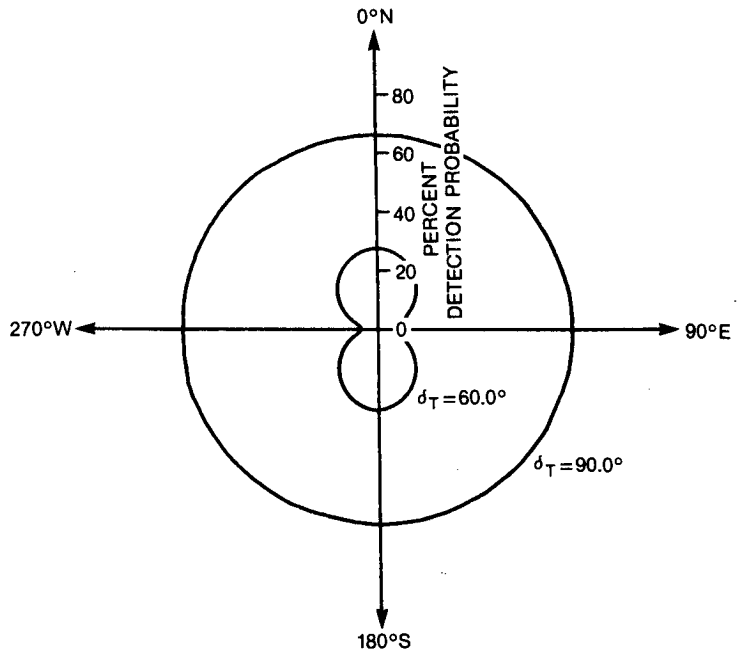

Figure 15 - Plots of the detection probabilities as a function of target target heading angle for target latitudes of 90.0° and 60.0°

For a target latitude of 90.0°, that is, a target positioned over the geometric north pole, the detection probability remained constant for all target headings. This constancy in the detection probability is reasonable since every orbit passes directly over the target and the antenna always has a look-ahead orientation. This results in an averaging over the same range of target radial velocities regardless of target heading. However, the results for the target latitude of 60.0° show a "pinching in" of the detection probability at headings of 90.0° and 270°.0. This is to be expected since, in general, the target's direction of motion is transverse to the orbital plane of the satellite resulting in small radial velocity components. Note that there is an overall reduction of the detection probabilities at the lower target latitude. This reduction arises because of greater variations in the look-direction, hence in less favourable directions for detection, and, on the average, a greater radar range to the target.

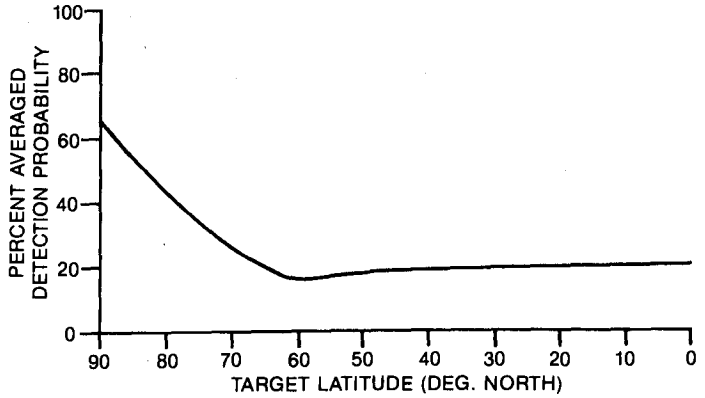

Figure 16 - Plot of the averaged detection probability against target latitude. Clutter reflectivity = -20.0 dBsm.

The detection probability averaged over all heading angles is shown as a function of target latitude in fig.(16). This result illustrates that, in general, the averaged detection probability decreased with decreasing target latitude. However, for latitudes less than 60.0°, a slight increase is observed. This arises because the average radar range to the target decreases slightly at these lower target latitudes.

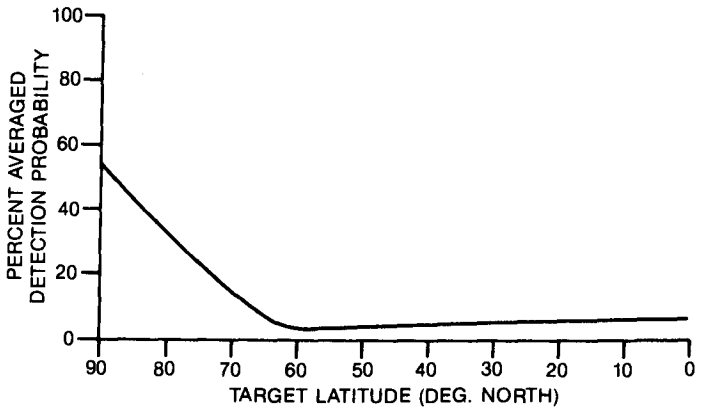

Figure 17 - Plot of the averaged detection probability against target latitude. Clutter reflectivity = -15.0 dBsm.

In fig.(17), a result is given of the averaged detection probability for the same experimental conditions as before except that the clutter reflectivity was raised to -15.0 dBsm. Again, the detection probability, in general, decreased with decreasing target latitude. Comparing this result to the result of fig.(16), we note that the detection probabilities are lower which is attributed to the increase in clutter

levels.

The results of these simulation studies are applicable to the evaluation of the detection performance of an SBR system, comprising a number of radar-satellites operating in circular polar orbits with the specified radar and satellite parameters.

11.0 SUMMARY AND CONCULSIONS

A description has been given of a computer-based analytical tool intended for the simulation of space-based radar systems for surveillance and tracking. This tool has been used to carry out studies of the detection performance of a baseline SBR system, using near-earth targets, in the presence of earth clutter. Several simplifying assumptions were incorporated into this simulator such as the assumption that the the earth-clutter reflectivity was constant, independent of terrain type and grazing angle. Notwithstanding these simplifying assumptions, it was possible to derive some general conclusions: (1) the clutter-velocity spectrum changes with every look-direction, (2) the detection performance of the SBR system decreases with decreasing target latitude for circular polar-orbiting satellites, and (3) the overall detection performance decreases with increasing clutter reflectivity.

12.0 ACKNOWLEDGEMENTS

Useful discussions with Dr. D. Faubert are acknowledged.

13.0 REFERENCES

1. Deutch, Ralph, "Orbital Dynamics of Space Vehicles", Prentice-Hall, 1963, pp. 9-11.

2. Deutch, ibid., pp. 12-16.

3. Deutch, ibid., pp. 10-11.

4. Rook, B.J., "Preliminary Coverage Studies for Space-based Radar Surveillance and Tracking", CRC Report No. 1363, August 1983.

5. Avrin, J.S., "Space-based Radar Prospects", Military Electronics/Countermeasures, Sept. 1981.

6. Bird, J.S. and A.W. Bridgewater, "Performance of Space-based Radar in the Presence of Earth Clutter", IEE Proceedings, Vol. 131, Pt. F, No. 5, August 1984.

7. Meyer, D.P. and H.A. Mayer, "Radar Target Detection - Handbook of Theory and Practice", Academic press, 1973.

8. Bird, J.S., "Calculating Detection Probabilities for Systems Employing Noncoherent Integration", IEEE Transaction on Aerospace and Electronic Systems, July 1982.

APPENDIX A

General Solution for θ and ϕ

From eqn.(46) in Section 4.4, the velocity of any point on the surface of the Earth relative to the satellite is given by

$$V = \left[V_{gs} \cos(\phi - \Delta) - V_e \cos \delta_s \sin \phi\right]\cos \gamma - \dot{r}\left[1 - \frac{r_e^2}{r^2} \cos^2\gamma \right]^{\frac{1}{2}} . \quad (A-1)$$

Given the values of i, δ_s and γ, we can solve eqn.(A-1) for ϕ by first specifying a velocity V. Since the value of γ is given, θ can be calculated by the geometrical relationships given by

$$\frac{\cos \theta}{r_e} = \frac{\cos \gamma}{r} . \quad (A-2)$$

Since for a given value of γ, the second term on the right-hand side of eqn.(A-1) is a constant for all ϕ, we may rewrite eqn.(A-1) as

$$V + C = \left[V_{gs} \cos(\phi - \Delta) - V_e \cos \delta_s \sin \phi\right]\cos \gamma \quad (A-3)$$

where

$$C = \dot{r}\left[1 - \frac{r_e^2}{r^2} \cos^2\gamma \right]^{\frac{1}{2}} . \quad (A-4)$$

Now, $\cos(\phi - \Delta) = \cos \phi \cos \Delta + \sin \phi \sin \Delta$, therefore,

$$V + C = V_{gs} \cos \gamma \cos \Delta \cos \phi - \left[V_e \cos \gamma \cos \delta_s - V_{gs} \cos \gamma \sin \Delta\right]\sin \phi . \quad (A-5)$$

Let

$$a = V_{gs} \cos \gamma \cos \Delta \quad (A-6)$$

and

$$b = V_e \cos \gamma \cos \delta_s - V_{gs} \cos \gamma \sin \Delta , \quad (A-7)$$

then

$$V + C = a \cos \phi - b \sin \phi . \quad (A-8)$$

By dividing through by $\left(a^2 + b^2\right)^{\frac{1}{2}}$ we have

$$\frac{V + C}{\left(a^2 + b^2\right)^{\frac{1}{2}}} = \cos A \cos \phi - \sin A \sin \phi = \cos(A + \phi) \quad (A-9)$$

where,

$$A = \arctan\left[\frac{b}{a}\right] \quad . \tag{A-10}$$

Since from eqn.(A-9)

$$\frac{V + C}{(a^2 + b^2)^{\frac{1}{2}}} = \cos(A + \phi) \quad , \tag{A-11}$$

then

$$\phi = \arccos\left[\frac{V + C}{(a^2 + b^2)^{\frac{1}{2}}}\right] - A \quad . \tag{A-12}$$

Replacing a, b and C by their expressions given by eqns.(A-6), (A-7) and (A-4) respectively yields

$$\phi = \arccos\left[\frac{V + \dot{r}\left[1 - \frac{r_e^2}{r^2}\cos^2\gamma\right]^{\frac{1}{2}}}{\left[(V_{gs}\cos\gamma\cos\Delta)^2 + (V_e\cos\gamma\cos\delta_s - V_{gs}\cos\gamma\sin\Delta)^2\right]^{\frac{1}{2}}}\right]$$

$$- \arctan\left[\frac{V_e\cos\delta_s - V_{gs}\sin\Delta}{V_{gs}\cos\Delta}\right] \quad . \tag{A-13}$$

For the special case of a circular polar orbit, that is, where the eccentricity e = 0, the inclination i = $\pi/2$, therefore cos $\Delta = \pm 1$, and

$$\dot{r} = 0, \tag{A-14}$$

$$r = a, \text{ a constant from eqn.(1)} \quad , \tag{A-15}$$

$$\dot{f} = \left[\frac{\mu}{r^3}\right]^{\frac{1}{2}} = \omega_s \quad , \tag{A-16}$$

$$V_{gs} = r_e\dot{f} = r_e\omega_s \quad , \tag{A-17}$$

then eqn.(A-5) reduces to

$$V = \pm V_{gs}\cos\gamma\cos\phi - V_e\cos\gamma\cos\delta_s\sin\phi \quad , \tag{A-18}$$

and eqn.(A-13) reduces to

$$\phi = \arccos\left[\frac{V}{\left((V_{gs}\cos\gamma)^2+(V_e\cos\gamma\cos\delta_s)^2\right)^{\frac{1}{2}}}\right] - \arctan\left[\frac{V_e\cos\delta_s}{\pm V_{gs}}\right]. \tag{A-19}$$

It should be noted that there are multiple solutions to the arc cos and arc tan functions and therefore care must be taken when evaluating eqns.(A-13) or (A-19).

UNCLASSIFIED

Security Classification

DOCUMENT CONTROL DATA - R & D

(Security classification of title, body of abstract and indexing annotation must be entered when the overall document is classified)

1. ORIGINATING ACTIVITY
Defence Research Establishment Ottawa
Department of National Defence
Ottawa, Ontario K1A 0Z4

2a. DOCUMENT SECURITY CLASSIFICATION
UNCLASSIFIED

2b. GROUP

3. DOCUMENT TITLE
Detection of Near-Earth Targets by Space-Based Radar: Development and Use of simulations

4. DESCRIPTIVE NOTES (Type of report and inclusive dates)
Report

5. AUTHOR(S) (Last name, first name, middle initial)
B.J. Rook, J.S. Bird and A.W. Bridgewater

6. DOCUMENT DATE	7a. TOTAL NO OF PAGES	7b. NO. OF REFS
July 1985	36	8

8a. PROJECT OR GRANT NO.	9a. ORIGINATOR'S DOCUMENT NUMBER(S)
33C87	CRC Report No. 1389
8b. CONTRACT NO.	9b. OTHER DOCUMENT NO.(S) (Any other numbers that may be assigned this document)

10. DISTRIBUTION STATEMENT
Unlimited

11. SUPPLEMENTARY NOTES	12. SPONSORING ACTIVITY
	DREO

13. ABSTRACT

A time-based computer simulation of space-based radar (SBR) systems is described. This simulator models the orbital dynamics of multiple radar satellites and the characteristics of the radar, and computes the clutter returns from the surface of the Earth as a function of Doppler velocity. It then determines the theoretical detectability of a target of specified radar cross-section, location and velocity at any given time.

The simulator has been used to carry out studies of the detection performance of a generic SBR system in a low-altitude polar orbit using near-earth targets in the presence of earth clutter. The results from these studies show that (1) the detection performance varies according to look-direction, and (2) the detection probabilities, in general, decrease with decreasing target latitude.

UNCLASSIFIED

Security Classification

KEY WORDS

Space Based Radar

INSTRUCTIONS

1. ORIGINATING ACTIVITY: Enter the name and address of the organization issuing the document.

2a. OOCUMENT SECURITY CLASSIFICATION: Enter the overall security classification of the document including special warning terms whenever applicable.

2b. GROUP: Enter security reclassification group number. The three groups are defined in Appendix 'M' of the DRB Security Regulations.

3. OOCUMENT TITLE: Enter the complete document title in all capital letters. Titles in all cases should be unclassified. If a sufficiently descriptive title cannot be selected without classification, show title classification with the usual one-capital-letter abbreviation in parentheses immediately following the title.

4. OESCRIPTIVE NOTES: Enter the category of document, e.g. technical report, technical note or technical letter. If appropriate, enter the type of document, e.g. interim, progress, summary, annual or final. Give the inclusive dates when a specific reporting period is covered.

5. AUTHOR(S): Enter the name(s) of author(s) as shown on or in the document. Enter last name, first name, middle initial. If military, show rank. The name of the principal author is an absolute minimum requirement.

6. OOCUMENT DATE: Enter the date (month, year) of Establishment approval for publication of the document.

7a. TOTAL NUMBER OF PAGES: The total page count should follow normal pagination procedures, i.e., enter the number of pages containing information.

7b. NUMBER OF REFERENCES: Enter the total number of references cited in the document.

8a. PROJECT OR GRANT NUMBER: If appropriate, enter the applicable research and development project or grant number under which the document was written.

8b. CONTRACT NUMBER: If appropriate, enter the applicable number under which the document was written.

9a. ORIGINATOR'S OOCUMENT NUMBER(S): Enter the official document number by which the document will be identified and controlled by the originating activity. This number must be unique to this document.

9b. OTHER DOCUMENT NUMBER(S): If the document has been assigned any other document numbers (either by the originator or by the sponsor), also enter this number(s).

10. DISTRIBUTiON STATEMENT: Enter any limitations on further dissemination of the document, other than those imposed by security classification, using standard statements such as:

    (1) "Qualified requesters may obtain copies of this document from their defence documentation center."

    (2) "Announcement and dissemination of this document is not authorized without prior approval from originating activity."

11. SUPPLEMENTARY NOTES: Use for additional explanatory notes.

12. SPONSORING ACTIVITY: Enter the name of the departmental project office or laboratory sponsoring the research and development. Include address.

13. ABSTRACT: Enter an abstract giving a brief and factual summary of the document, even though it may also appear elsewhere in the body of the document itself. It is highly desirable that the abstract of classified documents be unclassified. Each paragraph of the abstract shall end with an indication of the security classification of the information in the paragraph (unless the document itself is unclassified) represented as (TS), (S), (C), (R), or (U).

    The length of the abstract should be limited to 20 single-spaced standard typewritten lines; 7½ inches long.

14. KEY WORDS: Key words are technically meaningful terms or short phrases that characterize a document and could be helpful in cataloging the document. Key words should be selected so that no security classification is required. Identifiers, such as equipment model designation, trade name, military project code name, geographic location, may be used as key words but will be followed by an indication of technical context.